



Tailored Finite Point Method for Diffusion Equations with Interfaces on Distorted Meshes

Min Tang¹ · Lina Chang² · Yihong Wang³ 

Received: 17 April 2020 / Revised: 14 July 2021 / Accepted: 15 September 2021 /
Published online: 29 December 2021

© The Author(s), under exclusive licence to Springer Science+Business Media, LLC, part of Springer Nature 2021

Abstract

Diffusion processes is usually coupled with other physical processes such as the fluid equation. The meshes are determined by the fluid that can be distorted as time goes on. Classical finite difference schemes and finite element method are sensitive of mesh deformation. We propose a new tailored finite point method (TFPM) for 2D diffusion equation with tensor diffusion coefficient on highly distorted meshes. Second order convergence is demonstrated numerically with and without interfaces. TFPM is a finite difference method that makes full use of the analytical properties of local solutions. The main advantages of TFPM is that no modifications have to be made for problems with strongly discontinuous coefficients, where most other methods require special treatment at the interfaces. This advantage is important for distorted meshes, since the designing of numerical discretizations near interfaces is more delicate for distorted meshes.

Keywords Diffusion equation · Tailored Finite Point Method · Discontinuous diffusivity · Distorted mesh

M. Tang: This author is partially supported by NSFC 11301336 and 91330203.

Y. Wang: This author is partially supported by NSFC 11901393 and Natural Science Fund of Shanghai under the grant 19ZR1436300.

✉ Yihong Wang
wyh@lixin.edu.cn

Min Tang
tangmin@sjtu.edu.cn

Lina Chang
changln@iapcm.ac.cn

¹ Institute of natural sciences, MOE-LSC and department of mathematics, Shanghai Jiao Tong University, Shanghai 200240, China

² Institute of Applied Physics and Computational Mathematics, Beijing 100088, China

³ School of Statistics and mathematics, Shanghai Lixin University of Accounting and Finance, Shanghai 201209, China

1 Introduction

Diffusion processes are ubiquitous in physics, such as heat propagation or flows in porous media encountered in reservoir engineering [1], heat conduction in fusion plasma [2,3], atmospheric or oceanic flows [4], the radiation hydrodynamics [5]. In some applications, diffusion equation is usually coupled with fluid equations. The meshes are determined by the fluid that can be distorted as time goes on. Accurate and efficient numerical schemes for diffusion equations on distorted meshes are highly desired.

The stationary diffusion equation with tensor diffusion coefficients reads

$$\begin{cases} -\nabla \cdot (K \nabla u) = f, & \text{in } \Omega, \\ u = u_\Gamma, & \text{on } \partial\Omega, \end{cases} \quad (1)$$

where $\Omega \subset \mathbb{R}^2$ is the computational domain and $\partial\Omega$ is the boundary. The solution $u(x, y)$ is the temperature or pressure to be solved. The diffusion tensor $K(x, y)$ is a symmetric positive definite matrix that writes

$$K = \begin{pmatrix} K_{11} & K_{12} \\ K_{21} & K_{22} \end{pmatrix}. \quad (2)$$

There have been extensive research on developing numerical methods for stationary diffusion equation with tensor diffusion coefficients on general meshes, see reviews in [6–8]. Finite volume methods (FVM) are the most popular ones, the most recent FVM are not only stable and accurate for discontinuous and anisotropic diffusion tensors but also satisfying local mass conservation and discrete maximum principle on general distorted meshes [5,7,9–17]. Different FVM provides different way of constructing numerical fluxes at the cell faces. However, it is not easy to design high order schemes for FVM.

Discontinuous Galerkin methods [18–20] and finite element methods [21–25] are developed as well but much less works are available for distorted meshes. The problem of mesh-distortion sensitivity of finite element method, such as bilinear finite element methods on quadrilateral mesh, has been known to researchers for decades [26]. Mesh distortion leads to incorrect results or the interruption of computations. As discussed in [26,27], various new strategies have been proposed in order to improve the performance and robustness of traditional finite element methods when the meshes are distorted. The authors in [27] claimed that their method possess excellent precision in both regular and severely distorted meshes, even when a quadrilateral element degenerates into triangular or concave quadrangular shapes. That is the meaning of shape-free finite element. However, the analytical understanding of shape-free finite element methods is not clear. In [28] the authors provide the convergence analysis and error estimates for a mixed finite element method on distorted meshes. However, it is assumed that all the cells have comparable sizes, but their configurations may be quite different.

Classical finite difference schemes are only applicable to structured grids and the mimetic finite difference methods (MFD) possess excellent robustness in the presence of grid distortions and severe jumps in coefficients [29–33]. In MFD, it is crucial to find the discrete analog of some differential operators (for example, divergence or gradient) that can preserve some features of the operators at the continuous level. In this paper, we provide a new way of constructing finite difference schemes on distorted meshes. Similar to MFD, it uses solution properties at the continuous level to bypass the constraints of classical finite difference schemes, but the idea of scheme constructions is different from MFD.

Taylor finite point method (TFPM) was first proposed by Han, Huang and Kellogg for singular perturbed elliptic Eqs. [34] and has been extended to the non-homogeneous reaction-

diffusion, convection-diffusion, convection-diffusion-reaction, neutron transport equations and nonlinear radiation diffusion Eqs. [34–41]. The main idea of TFPM is to firstly approximate the diffusion coefficient near each grid by a constant, then use special solutions that satisfy exactly the diffusion equation with constant coefficients to determine the weights of a finite difference scheme. Since TFPMs make full use of analytical properties of local solutions, it can capture the boundary and interfaces layers with coarse meshes. However, all previous works of TFPM are on regular meshes and in this paper, we extend it to distorted meshes.

The extension is not trivial since the diffusion coefficients are no longer approximated by a constant near each grid, instead, the computational domain are divided into cells and the diffusion coefficients are approximated by piecewise linear functions inside each cell. The key point of the scheme construction is the discretization of the flux across cell edges. The common edge of two adjacent polygonal cells is denoted by Γ . The flux continuity on Γ can be written as

$$\mathbf{n}^+ \cdot K^+ \nabla u^+ = \mathbf{n}^- \cdot K^- \nabla u^-,$$

where u^\pm are localized solutions inside the two cells and \mathbf{n}^\pm are the out normal direction of Γ for u^\pm . Since u^\pm are approximated by a linear combination of special solutions, so are $\mathbf{n} \cdot K^\pm \nabla u^\pm$. Thus a discrete analog of flux continuity equation can be written down as well, using special solutions.

The main advantages of our proposed approach are that 1) all fluxes are localized, thus is appropriate for discontinuous and anisotropic diffusion tensors; 2) second order convergence with or without material discontinuities for general distorted meshes; 3) It preserves linear solutions for constant diffusion coefficients; 4) easy to code.

The paper is arranged as follows. In Sect. 2, we construct the TFPM on polygonal meshes. Several numerical examples on distorted meshes are presented in Sect. 3 and second order convergence is observed even when there are strong discontinuous diffusion tensors. Finally we conclude with some discussions in Sect. 4. In the appendix, we prove the second order convergence analytically for 1D TFPM. We would like to emphasis that the convergence does not depend on the ratio between the maximum and minimum mesh sizes, while most classical methods require lower bound for this ratio in the convergence proof.

2 The TFPM on General Polygonal Mesh

We use stencil as in Fig. 1. $\Omega_i (i = 1, 2 \dots, I)$ are I different polygon and the computational domain $\Omega = \bigcup_{i=1}^I \Omega_i$. $O_i = (x_i, y_i)$ stands for the center of gravity of Ω_i . The four edges and edge centers of Ω_i are respectively denoted by $\Gamma_{k,i}$ and $P_{k,i}, k = 1, 2, 3, 4$. Assume that the maximum length of $\Gamma_{k,i} (k = 1, 2, 3, 4)$ is h_i , and $h = \max\{h_i\}$.

In the subsequent part, we give details of the scheme construction, in which special solutions are used in each of the cell Ω_i and solutions of different cells are pieced together by the continuity of fluxes.

2.1 Approximated Special Solutions

On each Ω_i , we approximate Eq. (1) by

$$\begin{cases} -\nabla \cdot (\bar{K} \nabla \bar{u}) = \bar{f}, & \text{in } \Omega, \\ \bar{u} = u_\Gamma, & \text{on } \partial\Omega, \end{cases} \tag{3}$$

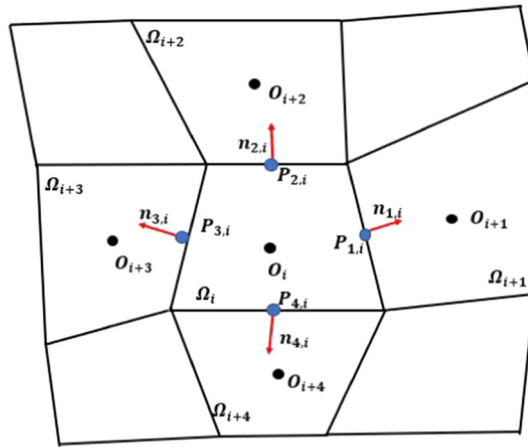


Fig. 1 TFSM stencil

where

$$\bar{K}|_{\Omega_i} = A_i(x - x_i) + B_i(y - y_i) + C_i, \quad \bar{f}|_{\Omega_i} = f_i + f_{x_i}(x - x_i) + f_{y_i}(y - y_i),$$

with

$$A_i = \begin{pmatrix} a_{11,i} & a_{12,i} \\ a_{21,i} & a_{22,i} \end{pmatrix}, \quad B_i = \begin{pmatrix} b_{11,i} & b_{12,i} \\ b_{21,i} & b_{22,i} \end{pmatrix}, \quad C_i = \begin{pmatrix} c_{11,i} & c_{12,i} \\ c_{21,i} & c_{22,i} \end{pmatrix},$$

being constant matrixes, (x_i, y_i) being the gravity center of Ω_i and f_i, f_{x_i}, f_{y_i} being constants. Here all 12 parameters in A_i, B_i and C_i are determined by $K_i(P_{k,i})$ ($k = 1, 2, 3, 4$), such that $\bar{K}(P_{k,i}) = K(P_{k,i})$; The constants f_i, f_{x_i}, f_{y_i} are respectively given by $f(x_i, y_i), \partial_x f(x_i, y_i)$ and $\partial_y f(x_i, y_i)$. $\bar{u}|_{\Omega_i}$ are pieced together by the continuity of \bar{u} and $\mathbf{n} \cdot \bar{K} \nabla \bar{u}$ at cell edges.

From the definitions of f_i, f_{x_i}, f_{y_i} , for $\forall i \in \{1, \dots, I\}$, when $f(x, y)|_{\Omega_i} \in C^2(\Omega_i)$,

$$f(x, y)|_{\Omega_i} = f(x_i, y_i) + (x - x_i)\partial_x f(x_i, y_i) + (y - y_i)\partial_y f(x_i, y_i) + O(h_i^2) = \bar{f}_i + O(h_i^2).$$

Then,

$$\|f - \bar{f}\|_2^2 = \sum_{i=1}^I \int_{\Omega_i} (f - \bar{f}_i)^2 dx \leq \sum_{i=1}^I C|\Omega_i|h_i^4 \leq C|\Omega|h^4. \tag{4}$$

Here $|\Omega_i|$ and $|\Omega|$ are the area of Ω_i and Ω . Therefore, $\|f - \bar{f}\|_2 \leq Ch^2$. Similarly, $\|K - \bar{K}\|_2 < Ch^2$. The difference between u and \bar{u} can be given by the following lemma.

Lemma 2.1 *Let $\bar{u} \in C^1(\Omega)$ and satisfy (3) in each interval Ω_i . Let $w = u - \bar{u}$, then*

$$\|\nabla w\|_2 < Ch^2, \quad \|w\|_2 < Ch^2. \tag{5}$$

Proof Since $w \in C^1(\Omega)$ and $w|_{\partial\Omega} = u|_{\partial\Omega} - \bar{u}|_{\partial\Omega} = u_\Gamma - u_\Gamma = 0$. Multiplying both sides of Eq. (1) by w and integrating over Ω , noting $w \in C^1(\Omega)$ and $w|_{\partial\Omega} = 0$, one gets

$$\int_{\Omega} (\nabla w) \cdot K \nabla u d\Omega = \int_{\Omega} w f d\Omega. \tag{6}$$

Similarly, from Eq. (3),

$$\int_{\Omega} (\nabla w) \cdot \bar{K} \nabla \bar{u} d\Omega = \int_{\Omega} w \bar{f} d\Omega. \tag{7}$$

Subtracting (6) from (7), one gets

$$\begin{aligned} \int_{\Omega} (\nabla w) \cdot K \nabla w d\Omega &= - \int_{\Omega} (\nabla w) \cdot (K - \bar{K}) \nabla \bar{u} d\Omega + \int_{\Omega} w (f - \bar{f}) d\Omega \\ &\leq \|\nabla w\|_2 \|(K - \bar{K}) \nabla \bar{u}\|_2 + \|w\|_2 \|f - \bar{f}\|_2, \end{aligned}$$

where the last inequality is from Holder’s inequality. Since $w \in C^1(\Omega)$ and $w|_{\partial\Omega} = 0$, from Friedrichs inequality we have $\|w\|_2 \leq C \|\nabla w\|_2$. Noting that K is positive definite and $\|K - \bar{K}\|_2 < Ch^2$, $\|f - \bar{f}\|_2 < Ch^2$, there exists C that is independent of h and satisfies

$$\|\nabla w\|_2 \leq Ch^2.$$

Then Friedrichs inequality gives

$$\|w\|_2 \leq C \|\partial_x w\|_2 \leq Ch^2.$$

□

The key idea of TFPM is to find special solutions inside each cell. However, since $\bar{K}|_{\Omega_i}$, $\bar{f}|_{\Omega_i}$ are linear functions in x and y , it is not easy to construct functions that satisfy exactly $-\nabla \cdot (\bar{K} \nabla \bar{u})|_{\Omega_i} = \bar{f}|_{\Omega_i}$. We then use some approximations that will not violate the scheme convergence.

Inside Ω_i , for any function \bar{v} ,

$$\begin{aligned} \nabla \cdot (\bar{K} \nabla \bar{v}) &= (a_{11,i} \partial_x^2 \bar{v} + a_{12,i} \partial_{xy} \bar{v} + a_{21,i} \partial_{xy} \bar{v} + a_{22,i} \partial_y^2 \bar{v})(x - x_i) + a_{11,i} \partial_x \bar{v} + a_{12,i} \partial_y \bar{v} \\ &\quad + (b_{11,i} \partial_x^2 \bar{v} + b_{12,i} \partial_{xy} \bar{v} + b_{21,i} \partial_{xy} \bar{v} + b_{22,i} \partial_y^2 \bar{v})(y - y_i) + b_{21,i} \partial_x \bar{v} + b_{22,i} \partial_y \bar{v} \\ &\quad + (c_{11,i} \partial_x^2 \bar{v} + c_{12,i} \partial_{xy} \bar{v} + c_{21,i} \partial_{xy} \bar{v} + c_{22,i} \partial_y^2 \bar{v}) \end{aligned}$$

We approximate $\nabla \cdot (\bar{K} \nabla \bar{v})|_{\Omega_i}$ and \bar{f}_i by

$$\nabla \cdot (\bar{K} \nabla \bar{v})|_{\Omega_i} \approx -r_{1,i} \partial_x^2 \bar{v} - r_{2,i} \partial_y^2 \bar{v} - r_{3,i} \partial_{xy}^2 \bar{v} - \beta_{1,i} \partial_x \bar{v} - \beta_{2,i} \partial_y \bar{v}, \quad \bar{f}_i|_{\Omega_i} \approx f_i, \tag{8}$$

where

$$\begin{aligned} r_{1,i} &= -c_{11,i}, \quad r_{2,i} = -c_{22,i}, \quad r_{3,i} = -c_{12,i} - c_{21,i}, \\ \beta_{1,i} &= -a_{11,i} - b_{21,i} \quad \beta_{2,i} = -a_{12,i} - b_{22,i}. \end{aligned}$$

Here, the terms dropped in Eq. (8) and in $\bar{f}_i|_{\Omega_i}$ are the terms at $O(h_i)$: $(a_{11,i} \partial_x^2 \bar{v} + a_{12,i} \partial_{xy} \bar{v} + a_{21,i} \partial_{xy} \bar{v} + a_{22,i} \partial_y^2 \bar{v})(x - x_i)$, $(b_{11,i} \partial_x^2 \bar{v} + b_{12,i} \partial_{xy} \bar{v} + b_{21,i} \partial_{xy} \bar{v} + b_{22,i} \partial_y^2 \bar{v})(y - y_i)$, and $f_{xi}(x - x_i) + f_{yi}(y - y_i)$. Inside Ω_i , \bar{u}_h satisfies

$$r_{1,i} \partial_x^2 \bar{u}_h + r_{2,i} \partial_y^2 \bar{u}_h + r_{3,i} \partial_{xy}^2 \bar{u}_h + \beta_{1,i} \partial_x \bar{u}_h + \beta_{2,i} \partial_y \bar{u}_h = f_i. \tag{9}$$

Then

$$\nabla \cdot (\bar{K}_i \nabla \bar{u}_h) + \bar{f}_i = R.H.S. \tag{10}$$

with

$$\begin{aligned} R.H.S. &= (a_{11} \partial_x^2 \bar{u}_h + a_{12} \partial_{xy} \bar{u}_h + a_{21} \partial_{xy} \bar{u}_h + a_{22} \partial_y^2 \bar{u}_h)(x - x_i) \\ &\quad + (b_{11} \partial_x^2 \bar{u}_h + b_{12} \partial_{xy} \bar{u}_h + b_{21} \partial_{xy} \bar{u}_h + b_{22} \partial_y^2 \bar{u}_h)(y - y_i) \\ &\quad + f_{xi}(x - x_i) + f_{yi}(y - y_i). \end{aligned}$$

Since (x_i, y_i) is the center of Ω_i such that $\frac{1}{|\Omega_i|} \int_{\Omega_i} x \, dx \, dy = x_i, \frac{1}{|\Omega_i|} \int_{\Omega_i} y \, dx \, dy = y_i$, from $\bar{u}_h|_{\Omega_i} \in C^\infty(\Omega_i)$, we have

$$\int_{\Omega_i} R.H.S. \, dx \, dy = O(h_i^4).$$

We now find special solutions to (9). If $\beta_{1,i} = \beta_{2,i} = 0$, the general solution to Eq. (9) can be written as

$$\bar{u}_{hi}(x, y) = \tilde{v}_i(x, y) + v_i(x, y). \tag{11}$$

Let $\tilde{v}_i(x, y) = \frac{r_{1,i}(x-x_i)^2+r_{2,i}(y-y_i)^2}{2(r_{1,i}^2+r_{2,i}^2)} f_i$. It is the special solution of Eq. (9) and $v_i(x, y)$ satisfies the homogenous equation

$$r_{1,i} \frac{\partial^2 v_i}{\partial x^2} + r_{2,i} \frac{\partial^2 v_i}{\partial y^2} + r_{3,i} \frac{\partial^2 v_i}{\partial x \partial y} = 0. \tag{12}$$

Otherwise, when $\beta_{1,i}^2 + \beta_{2,i}^2 > 0$, the special solution of Eq. (9) becomes $\tilde{v}_i(x, y) = \frac{\beta_{1,i}(x-x_i)+\beta_{2,i}(y-y_i)}{(\beta_{1,i}^2+\beta_{2,i}^2)} f_i$ and $v_i(x, y)$ satisfies the homogenous equation

$$r_{1,i} \frac{\partial^2 v_i}{\partial x^2} + r_{2,i} \frac{\partial^2 v_i}{\partial y^2} + r_{3,i} \frac{\partial^2 v_i}{\partial x \partial y} + \beta_{1,i} \frac{\partial v_i}{\partial x} + \beta_{2,i} \frac{\partial v_i}{\partial y} = 0. \tag{13}$$

We choose 4 linearly independent functions $W_{k,i} (k = 1, 2, 3, 4)$ that satisfy the homogeneous equation and approximate $v(x, y)|_{\Omega_i}$ by a function belonging to the linear space

$$H_i = \left\{ \sum_{k=1}^n c_{k,i} W_{k,i}, \quad c_{k,i} \in \mathbb{R} \right\}. \tag{14}$$

where $c_{k,i}$ are constant coefficients inside Ω_i .

In order to find $W_{k,i}$, suppose $v_i(x, y)$ is of the special form

$$v_i(x, y) = e^{\lambda x + \mu y}. \tag{15}$$

Then v_i of the form as in (15) satisfies (13) when (λ, μ) is the solution to

$$r_{1,i} \lambda^2 + r_{2,i} \mu^2 + r_{3,i} \lambda \mu + \beta_{1,i} \lambda + \beta_{2,i} \mu = 0. \tag{16}$$

We choose $(\lambda, \mu) = (-\frac{\beta_{1,i}}{r_{1,i}}, 0), (0, -\frac{\beta_{2,i}}{r_{2,i}})$. Next, we find solution of the form

$$v_i(x, y) = (a_{0,i}x + b_{0,i}y)e^{\lambda x + \mu y}. \tag{17}$$

Substituting the above form into (13) yields

$$a_{0,i} = -(2r_{2,i}\mu + r_{3,i}\lambda + \beta_{2,i}), \quad b_{0,i} = (2r_{1,i}\lambda + r_{3,i}\mu + \beta_{1,i}).$$

Therefore, we choose $W_{k,i}$ are of the following form:

Case 1 $\beta_{1,i}^2 + \beta_{2,i}^2 = 0$:

$$W_{1,i}(x, y) = 1, \quad W_{2,i}(x, y) = x, \quad W_{3,i}(x, y) = y, \quad W_{4,i}(x, y) = r_{2,i}x^2 - r_{1,i}y^2. \tag{18}$$

Case 2 $\beta_{1,i}^2 + \beta_{2,i}^2 \neq 0$:

$$\begin{aligned}
 W_{1,i}(x, y) &= e^{-\frac{\beta_{1,i}}{r_{1,i}}x}, & W_{2,i}(x, y) &= e^{-\frac{\beta_{2,i}}{r_{2,i}}y}, \\
 W_{3,i}(x, y) &= \left(\left(\frac{r_{3,i}\beta_{1,i}}{r_{1,i}} - \beta_{2,i} \right) x - \beta_{1,i}y \right) e^{-\frac{\beta_{1,i}}{r_{1,i}}x}, \\
 W_{4,i}(x, y) &= \left(\beta_{2,i}x + \left(\frac{-r_{3,i}\beta_{2,i}}{r_{2,i}} + \beta_{1,i} \right) y \right) e^{-\frac{\beta_{2,i}}{r_{2,i}}y}.
 \end{aligned} \tag{19}$$

If $\beta_{1,i} \rightarrow 0, \beta_{2,i} \neq 0$, then $W_{1,i}(x, y) \rightarrow 1, W_{3,i}(x, y) \rightarrow -\beta_{2,i}x$. If $\beta_{2,i} \rightarrow 0, \beta_{1,i} \neq 0$, then $W_{2,i}(x, y) \rightarrow 1, W_{4,i}(x, y) \rightarrow \beta_{1,i}y$. $W_{k,i}$ in (19) are independent functions.

2.2 Construction of TFPM

As discussed in sect. 2.1, the solution to (3) inside each cell Ω_i is approximated by

$$\bar{u}_i(x, y) \approx \sum_{k=1}^4 c_{k,i} W_{k,i} + \tilde{v}_i \tag{20}$$

and the derivatives of v_i can be obtained analytically such that

$$\partial_x \bar{u}_i(x, y) \approx \sum_{k=1}^4 c_{k,i} \partial_x W_{k,i} + \partial_x \tilde{v}_i, \quad \partial_y \bar{u}_i(x, y) \approx \sum_{k=1}^4 c_{k,i} \partial_y W_{k,i} + \partial_y \tilde{v}_i. \tag{21}$$

We construct the TFPM by the continuity of fluxes in two adjacent cells. For all cells, denote

$$\bar{u}|_{\Omega_i} = \bar{u}_i, \quad \bar{K}|_{\Omega_i} = \bar{K}_i.$$

Assume that Ω_i and Ω_{i+1} are two adjacent cells and their common edge is $\Gamma_{1,i}$, then the continuity of \bar{u} and $\mathbf{n} \cdot \bar{K} \nabla \bar{u}$ on $\Gamma_{1,i}$ write

$$\begin{cases} \bar{u}_i(x, y)|_{\Gamma_{1,i}} = \bar{u}_{i+1}(x, y)|_{\Gamma_{1,i}}, \\ \mathbf{n}_{1,i} \cdot \bar{K}_i(x, y) \nabla \bar{u}_i(x, y)|_{\Gamma_{1,i}} = -\mathbf{n}_{1,i+1} \cdot \bar{K}_{i+1}(x, y) \nabla \bar{u}_{i+1}(x, y)|_{\Gamma_{1,i}}, \end{cases} \tag{22}$$

where $\mathbf{n}_{1,i}$ ($\mathbf{n}_{1,i+1}$) is out normal direction of Ω_i (Ω_{i+1}) perpendicular to $\Gamma_{1,i}$. When $\bar{u}_i(x, y), \partial_x \bar{u}_i(x, y)$ and $\partial_y \bar{u}_i(x, y)$ are respectively approximated by $\bar{v}_i(x, y), \partial_x \bar{v}_i(x, y)$ and $\partial_y \bar{v}_i(x, y)$ as in (20), (21), the continuity Eq. (22) can no longer be satisfied at all points on $\Gamma_{1,i}$. Since there exist only a finite number of basis, the solution and fluxes can only be continuous at a finite number of points on $\Gamma_{1,i}$. Therefore, we piece together \bar{v}_i and \bar{v}_{i+1} at the center of $\Gamma_{1,i}$. As in Fig. 1, the middle point of $\Gamma_{1,i}$ is $P_{1,i}$ whose coordinates are $(x_{1,i}, y_{1,i})$, the continuity conditions at $P_{1,i}$ write:

$$\sum_{k=1}^4 c_{k,i} W_{k,i}(x_{1,i}, y_{1,i}) + \tilde{v}_i = \sum_{k=1}^4 c_{k,i+1} W_{k,i+1}(x_{1,i}, y_{1,i}) + \tilde{v}_{i+1} \tag{23a}$$

$$\begin{aligned} \mathbf{n}_{1,i} \cdot \left(\bar{K}_i \left(\sum_{k=1}^4 c_{k,i} \nabla W_{k,i} + \nabla \tilde{v}_i \right) \right) (x_{1,i}, y_{1,i}) \\ = \mathbf{n}_{1,i} \cdot \left(\bar{K}_{i+1} \left(\sum_{k=1}^4 c_{k,i+1} \nabla W_{k,i+1} + \nabla \tilde{v}_{i+1} \right) \right) (x_{1,i}, y_{1,i}). \end{aligned} \tag{23b}$$

A finite difference scheme can be derived from the above continuity conditions. Assume that there are I polygon cells in the computational domain and J cell edges at the boundary. Then there are $(4I - J)/2$ edges inside the computational domain. Let $c_{k,i}$ be the unknowns and in order to determine the $4I$ unknowns, $4I$ equations are required. (23) gives two equations for each cell edge inside the computational domain, which yields $4I - J$ equations. For each cell edge Γ_{bi} at the boundary, assume that it belongs to the cell Ω_i . Let $P_{bi} = (x_{bi}, y_{bi})$ be the edge center, Dirichlet boundary conditions write

$$\sum_{k=1}^4 c_{k,i} W_{k,i}(x_{bi}, y_{bi}) + \tilde{v}_i(x_{bi}, y_{bi}) = u(x_{bi}, y_{bi}). \tag{24}$$

which gives J equations. Therefore, we have a system of $4I$ linear algebraic equations and the $4I$ coefficients $c_{k,i}$ can be determined. The linear system is four times bigger than the FVM and double the size of MFDM, thus is not efficient enough.

Another way of constructing the scheme is to let the unknowns be solution values at all edge centers. There are $2I + J/2$ edge centers in the computational domain. let $u_{k,i} \approx u(x_{k,i}, y_{k,i})$ ($k = 1, 2, 3, 4$), when $u_i(x, y)$ are approximated as in (20), $u_{k,i}$ can determine the coefficients $c_{k,i}$ by the following system

$$\begin{cases} \sum_{k=1}^4 c_{k,i} W_{k,i}(x_{1,i}, y_{1,i}) + \tilde{v}_i(x_{1,i}, y_{1,i}) = u_{1,i}, \\ \sum_{k=1}^4 c_{k,i} W_{k,i}(x_{2,i}, y_{2,i}) + \tilde{v}_i(x_{2,i}, y_{2,i}) = u_{2,i}, \\ \sum_{k=1}^4 c_{k,i} W_{k,i}(x_{3,i}, y_{3,i}) + \tilde{v}_i(x_{3,i}, y_{3,i}) = u_{3,i}, \\ \sum_{k=1}^4 c_{k,i} W_{k,i}(x_{4,i}, y_{4,i}) + \tilde{v}_i(x_{4,i}, y_{4,i}) = u_{4,i}. \end{cases} \tag{25}$$

Therefore, the continuity of fluxes in (23b) can be expressed by $u_{k,i}$ and $u_{k,i+1}$ ($k = 1, 2, 3, 4$) which yields $2I - J/2$ equations. Together with the J equations given by Dirichlet boundary conditions, one can get $2I + J/2$ equations for the $2I + J/2$ unknowns. In this way, the computational efficiency is the same as MFDM.

3 Numerical Experiments

The performance of the the new TFPM on some highly skewed and highly distorted meshes are presented in this section. Three different kinds of distorted meshes are tested: Kershaw, Shestakov and random. As shown in Figs. 2, 3, 4, a typical Kershaw mesh has a large distortion in vertical direction, a typical Shestakov mesh has three non-convex cells and the random mesh is obtained by randomly disturbing the interior mesh vertices of the uniform mesh. These meshes have been used to test scheme performances on unstructured or highly distorted meshes in the literature [42,43]. In all examples, let the computational domain

Table 1 The number of cells are used to test the convergence order

Mesh	Cells				
Kershaw	20 × 20	40 × 40	80 × 80	160 × 160	320 × 320
Shestakov	16 × 16	32 × 32	64 × 64	128 × 128	256 × 256
Random	20 × 20	40 × 40	80 × 80	160 × 160	320 × 320

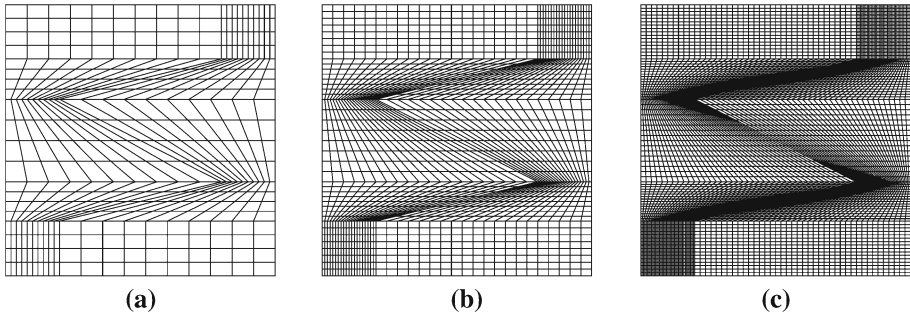


Fig. 2 Kershaw meshes. **a** 20 × 20; **b** 40 × 40; **c** 80 × 80

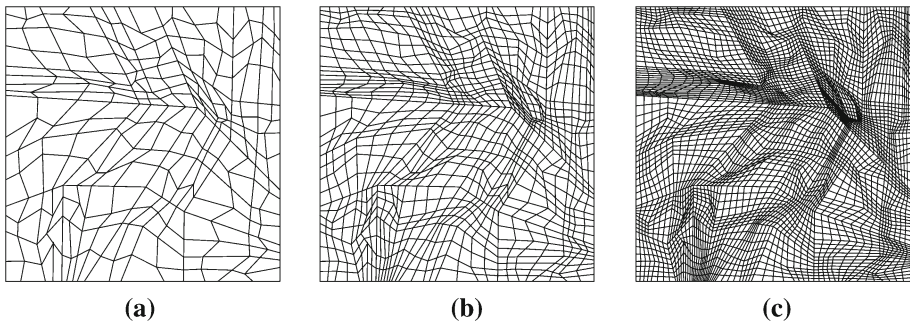


Fig. 3 Shestakov meshes. **a** 16 × 16; **b** 32 × 32; **c** 64 × 64

be $\Omega = [0, 1] \times [0, 1]$. To obtain the convergence order of L^2 error estimates for the first two examples, the number of cells of the three kinds of distorted meshes are displayed on Table 1.

Kershaw, Shestakov meshes are refined in a nested manner. Please see Figs. 2 and 3. For the random meshes, it is constructed from a uniform square mesh of size h and then randomly move the nodes (x, y) to a new position $(x + \omega\xi_x h/2, y + \omega\xi_y h/2)$. Here ξ_x and ξ_y are random numbers uniformly distributed in $[-0.5, 0.5]$ and $\omega \in [0, 1]$ is a constant referred as "the degree of distortion". The meshes are still skewed or even deteriorate as they are refined. As shown in Fig. 4.

Example 1 In this example we test the scheme accuracy and convergence order for anisotropic diffusion tensor:

$$K = \begin{pmatrix} \cos \theta & \sin \theta \\ -\sin \theta & \cos \theta \end{pmatrix} \begin{pmatrix} \frac{1}{\epsilon} & 0 \\ 0 & 1 \end{pmatrix} \begin{pmatrix} \cos \theta & -\sin \theta \\ \sin \theta & \cos \theta \end{pmatrix}, \tag{26}$$

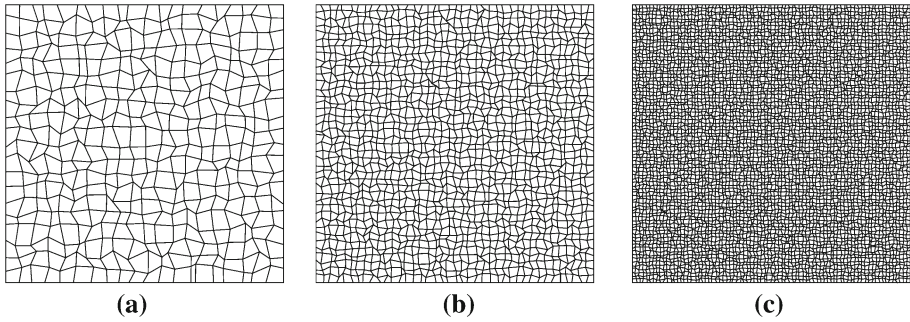


Fig. 4 Random meshes with the degree of distortion $\omega = 0.7$. **a** 20×20 ; **b** 40×40 ; **c** 80×80

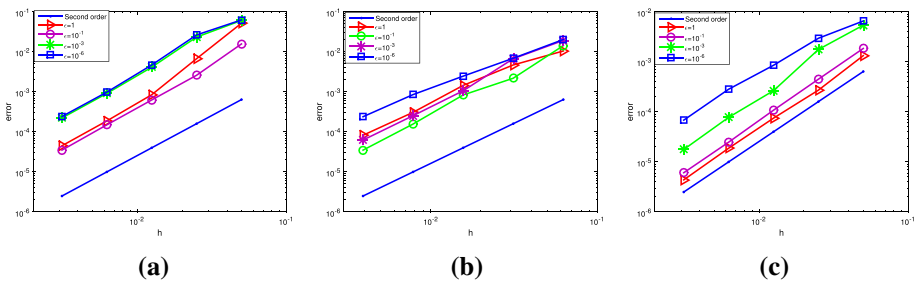


Fig. 5 Example 1. The L^2 norm of errors for different meshes and ϵ values of the new TFPM. **a** Kershaw meshes; **b** Shestakov meshes **c** Random meshes

with $\theta = 40^\circ$. The exact solution is $u_{exact} = xy(\sin(\pi x) \sin(\pi y))^{10}$ and the source term f and boundary conditions are chosen according to the exact solution. As shown in Fig. 5, second order convergence can be observed for all three kinds of distorted meshes in Fig. 2.

Example 2 Space varying diffusion tensor is tested in this example. K is chosen to be an anisotropic rotating tensor such that

$$K = \begin{pmatrix} 10x^2 + y^2 & 9xy \\ 9xy & x^2 + 10y^2 \end{pmatrix},$$

We impose the following exact solution

$$u = \exp(-20\pi((x - 0.5)^2 + (y - 0.5)^2)).$$

The source term and boundary conditions are determined by substituting u into (1). As shown in Fig. 6, TFPM exhibits second order convergence for all three types of meshes when the diffusion tensors vary in space. We can see from Figs. 3 and 4 that in the Shestakov mesh and Random mesh, some quadrilateral element degenerates into triangular, but the convergence order remains.

Example 3 In this example we solve an interface problem. The computational domain Ω is divided into two subdomains: $[0, 0.5] \times [0, 1]$ and $[0.5, 1] \times [0, 1]$. Each has a different diffusion tensor such that

$$K(x, y) = \begin{pmatrix} 10 & 2 \\ 2 & 5 \end{pmatrix} \text{ for } x \leq 0.5, \quad K(x, y) = \begin{pmatrix} 10^3 & 0 \\ 0 & 1 \end{pmatrix} \text{ for } x > 0.5.$$

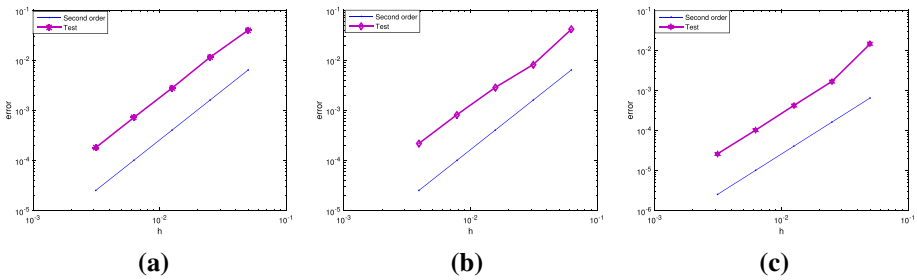


Fig. 6 Example 2. The L^2 norm of errors for different distorted meshes of TFPM. **a** Kershaw meshes; **b** Shestakov meshes; **c** Random meshes

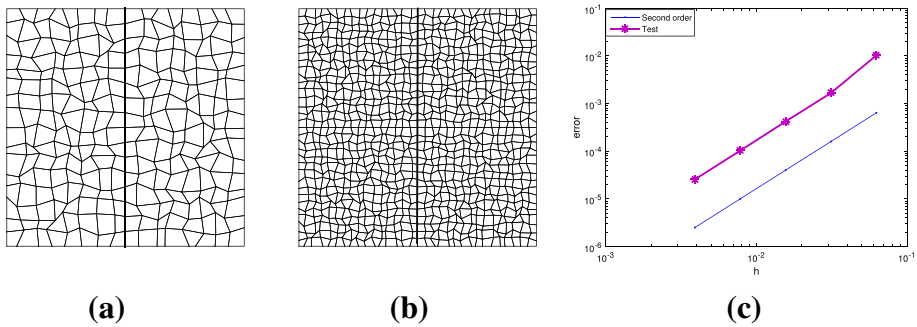


Fig. 7 Example 3. Random meshes with the degree of distortion $\omega = 0.7$. **a** $I = 16^2$; **b** $I = 32^2$; **c** Convergence order of the TFPM for problem with interface on random meshes

Random meshes are used in each subdomain. The analytical solution is defined as follows:

$$u(x, y) = \begin{cases} [1 + (x - 0.5)(0.1 + 8\pi(y - 0.5))]e^{-20\pi(y-0.5)^2} & x \leq 0.5, \\ e^{\frac{x-0.5}{10^3}} e^{-20\pi(y-0.5)^2} & x > 0.5. \end{cases} \tag{27}$$

The source term f and boundary conditions are chosen according to the exact solution. The solution is continuous but its derivatives are discontinuous at the interface. For this test problem, two different meshes are tested. Random meshes are refined by the degree of distortion $\omega = 0.7$ and trapezoidal meshes are refined in a self-similar fashion as in [21,22]. As in Figs. 7, 8, second order convergence in the L^2 norm can be observed numerically for the solution. Different from the bilinear finite element methods, no decreasing of convergence order is observed when trapezoidal meshes are refined.

Example 4 In this example, we consider a more complicate case when the unit square $[0, 1] \times [0, 1]$ is split into four subdomains: $\Omega_1 = [0, \frac{1}{2}] \times [0, \frac{1}{2}]$, $\Omega_2 = [\frac{1}{2}, 1] \times [0, \frac{1}{2}]$, $\Omega_3 = [\frac{1}{2}, 1] \times [\frac{1}{2}, 1]$, $\Omega_4 = [0, \frac{1}{2}] \times [\frac{1}{2}, 1]$. The source term is defined by

$$f(x, y) = \begin{cases} \frac{81}{4}, & \text{for } x \in [\frac{7}{18}, \frac{11}{18}]^2, \\ 0, & \text{otherwise.} \end{cases} \tag{28}$$

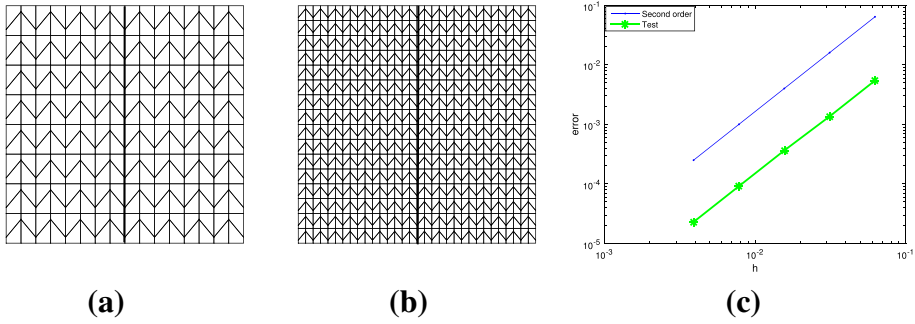


Fig. 8 Example 3. Meshes of self-similar trapezoids. **a** $I = 16^2$; **b** $I = 32^2$; **c** Convergence order of the TFPM for problem with interface on trapezoidal meshes

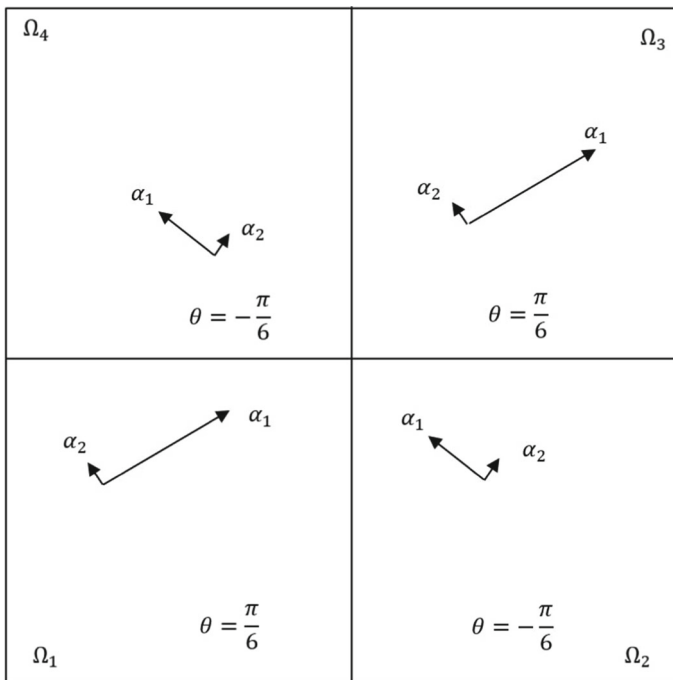


Fig. 9 Example 4. An illustration of subdomain together with a synoptic description of the diffusivity tensor

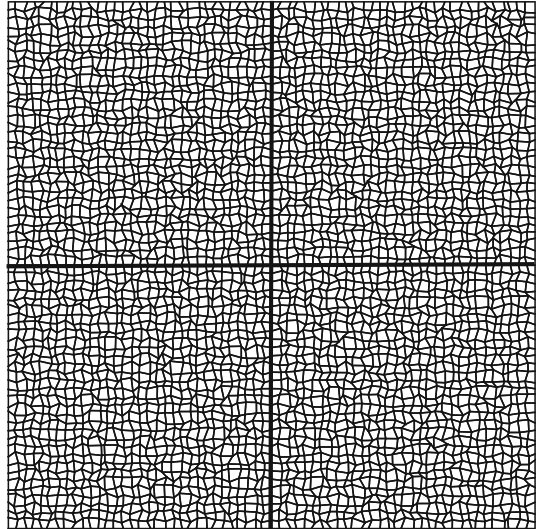
As in Fig. 9, there are two interfaces along $x = 1/2$ and $y = 1/2$, the diffusion tensors in the subdomains are given by

$$K(x, y) = \begin{pmatrix} \cos \theta & -\sin \theta \\ \sin \theta & \cos \theta \end{pmatrix} \begin{pmatrix} \alpha_1 & 0 \\ 0 & \alpha_2 \end{pmatrix} \begin{pmatrix} \cos \theta & \sin \theta \\ -\sin \theta & \cos \theta \end{pmatrix}, \text{ for } (x, y) \in \Omega_1, \Omega_3 \quad (29)$$

with $\theta = \pi/6$ and

$$K(x, y) = \begin{pmatrix} \cos \theta & -\sin \theta \\ \sin \theta & \cos \theta \end{pmatrix} \begin{pmatrix} \alpha_1 & 0 \\ 0 & \alpha_2 \end{pmatrix} \begin{pmatrix} \cos \theta & \sin \theta \\ -\sin \theta & \cos \theta \end{pmatrix}, \text{ for } (x, y) \in \Omega_2, \Omega_4 \quad (30)$$

Fig. 10 Example 4. Random meshes with the degree of distortion $\omega = 0.7$ are used on each side of the interface



with $\theta = -\pi/6$. Random mesh as in Fig. 10 are tested. Two cases are considered. Case 1: $\alpha_1 = 10^3$, $\alpha_2 = 10$ in Ω_1, Ω_3 , $\alpha_1 = 10$, $\alpha_2 = 1$ in Ω_2, Ω_4 . Case 2: $\alpha_1 = 10^6$, $\alpha_2 = 10^3$ in Ω_1, Ω_3 , $\alpha_1 = 10$, $\alpha_2 = 1$ in Ω_2, Ω_4 . To demonstrate the robustness of the proposed TFPM method, we present the numerical results with the resolution of 64^2 , 128^2 , 256^2 and 512^2 in this example. See Figs. 11, 12. The TFPM can capture fast changes at the interfaces. The corresponding CPU time for each resolution also be reported in Table 2.

4 Conclusion

TFPM for anisotropic and strong discontinuous diffusivity problems on distorted meshes is constructed in this paper. First of all, the computational domain is divided into unstructured cells, inside each cell, the diffusion coefficients are approximated by piecewise linear functions. Then special solutions to an approximated constant coefficient advection-diffusion equation are used to construct the discrete analog of flux continuity equation. The local stencil makes it easy to code. The scheme can achieve second order convergence for problems with or without material discontinuities. Compared with MFDM, the number of unknowns are the same, both methods use properties of continuum solutions and seem robust for distorted meshes, it is interesting to investigate the relation between the two approaches, which will be our future work.

The new discrete scheme is an edge-centered scheme. The function values at the cell centers or vertexes or other auxiliary unknowns are not needed to construct the discrete normal flux. The out normal flux of each cell can be expressed by the unknowns at cell edge centers of the local cell, while no information from adjacent cells is needed. So it is suitable for problems with interfaces and for meshes with complex geometry. Numerical examples show that the order of convergence for the TFPM is about 2. No decreasing of convergence order is observed when the skewed meshes and trapezoidal meshes are refined. Since we are considering the distorted meshes, the convergence order analysis is difficult for general 2D

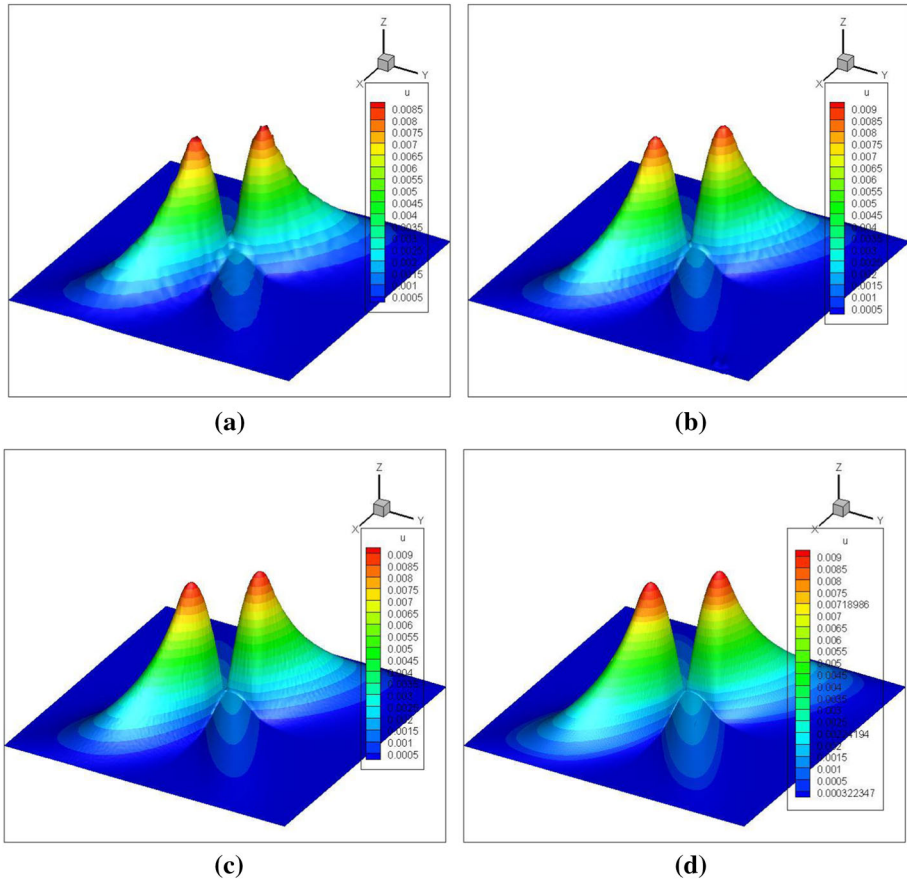


Fig. 11 Example 4. Case 1 **a** Random meshes 64×64 ; **b** Random meshes 128×128 ; **c** 256×256 ; **d** 512×512

case. We give a second order convergence proof for a 1D TFPM in appendix. We would like to emphasize two aspects that the 1D proof may inspire:

- By letting h_i be the length of the i th mesh, the convergence order is independent of $\max\{h_i\}/\min\{h_i\}$. This implies that very non-uniform meshes do not ruin the convergence order. Most classical numerical methods like finite element, finite volume etc., the convergence order depends on the ratio $\max\{h_i\}/\min\{h_i\}$ [7,22].
- It is not easy to construct functions that exactly satisfy $-\nabla \cdot (\bar{K} \nabla \bar{u})|_{\Omega_i} = \bar{f}|_{\Omega_i}$. So we use some approximations to $\nabla \cdot (\bar{K} \nabla \bar{u})|_{\Omega_i}$ and $\bar{f}|_{\Omega_i}$. The terms dropped in Eq. (8) and in $\bar{f}|_{\Omega_i}$ are terms at $O(h)$. We can understand from the 1D convergence order analysis that why second order convergence remains after dropping these terms.

We are not able to prove analytically the second order convergence of TFPM for general 2D distorted meshes in this current paper, but it will be our future work.

Higher order extension of the TFPM is possible, but more unknowns at each cell edge are needed (values at other points or the solution derivatives at the cell edge). The fourth order long-stencil finite difference algorithm has used larger stencil [44,45] and the higher order version of TFPM would be different from fourth order long-stencil finite difference.

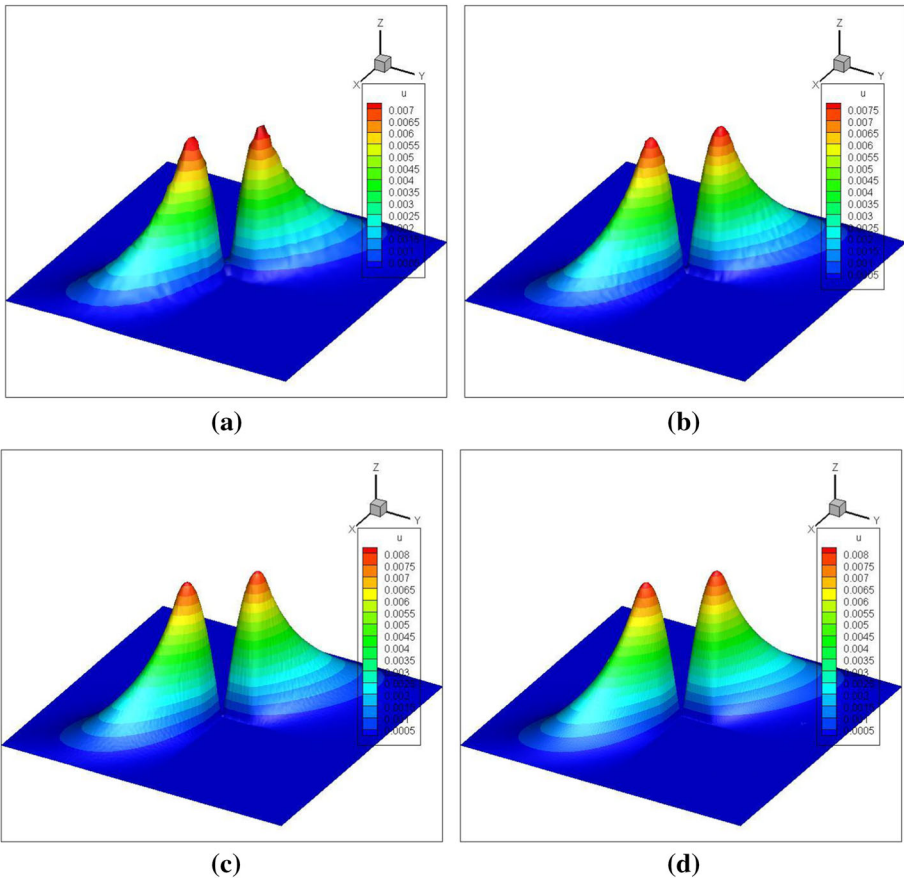


Fig. 12 Example 4. Case 2 **a** Random meshes 64×64 ; **b** Random meshes 128×128 ; **c** 256×256 ; **d** 512×512

Table 2 Example 4. The CPU time for each resolution

Mesh size	64×64	128×128	256×256	512×512
Case 1	1.875s	25.313s	590.828s	10831.656s
Case 2	1.875s	29.406s	704.812s	10880.297s

CRediT Authorship Contribution Statement

Min Tang: Conceptualization, Methodology, Validation, Writing-original draft, Writing -review & editing. **Lina Chang:** Software, Validation, Writing-review & editing. **Yihong Wang:** Investigation, Methodology, Validation, Software, Writing-original draft, Writing -review & editing.

Acknowledgements The authors thank the anonymous reviewers for their careful readings and useful suggestions.

Appendix: Convergence Analysis for 1D Case

We give the convergence order analysis for the 1D case to present the main ideas of the convergence order analysis.

1D TFPM

Let the computational domain be $[0, L]$ and $K(x) \in C^1[0, L]$ be a scalar function that satisfies $0 < \zeta_1 < K_1(x) < \zeta_2$, we consider the following 1D diffusion equation:

$$\begin{cases} -\partial_x(K(x)\partial_x u) = f, & x \in (0, L) \\ u(0) = u_0, & u(L) = u_L. \end{cases} \tag{31}$$

In this subsection, without any confusion, we use the same notations for the diffusion coefficient and solution as for 2D TFPM.

Let the stencil be as in Fig. 13. The interval $[0, L]$ is divided into I sub-intervals that are denoted by $L_i = [x_{i-1}, x_i]$ with $i = 1, 2, \dots, I$ and $x_0 = 0, x_I = L$. Let $x_{i-1/2} = \frac{x_i+x_{i-1}}{2}$ be the center of L_i and $h_i = x_i - x_{i-1}$ be the length of i th interval. On L_i , (31) can be approximated by

$$-\partial_x(\bar{K}_i(x)\partial_x \bar{u}) = \bar{f}_i, \tag{32}$$

where

$$\bar{K}_i(x) = k_{xi}(x - x_{i-1/2}) + k_i, \quad \text{with} \quad k_i = \frac{K(x_{i-1}) + K(x_i)}{2} \quad \text{and} \quad k_{xi} = \frac{K(x_i) - K(x_{i-1})}{h_i}, \tag{33}$$

and

$$\bar{f}_i = f_i + f_{xi}(x - x_{i-1/2}) \quad \text{with} \quad f_i = \frac{f(x_{i-1}) + f(x_i)}{2} \quad \text{and} \quad f_{xi} = \frac{f(x_i) - f(x_{i-1})}{h_i}. \tag{34}$$

Piecing $\bar{K}_i(x)$ together gives $\bar{K} \in C[0, L]$. If we piece $\bar{u}|_{L_i}$ together by the continuity of \bar{u} and $\bar{K}(x)\partial_x \bar{u}$ at the grid points, we find an approximation to the solution of (31).

Let

$$\tilde{v}_i(x) = \begin{cases} -\frac{x-x_{i-1/2}}{k_{xi}} f_i, & k_{xi} \neq 0, & W_{1,i}(x) = 1, & W_{2,i}(x) = e^{-\frac{k_{xi}(x-x_{i-1/2})}{k_i}}, & k_{xi} \neq 0, \\ -\frac{(x-x_{i-1/2})^2}{2k_i} f_i, & k_{xi} = 0, & W_{1,i}(x) = 1, & W_{2,i}(x) = x, & k_{xi} = 0. \end{cases} \tag{35}$$

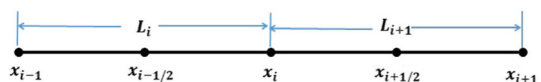
Then for any constants c_{1i}, c_{2i} , $u_{hi}(x) = \sum_{k=1}^2 c_{ki} W_{k,i}(x) + \tilde{v}_i(x)$ exactly satisfies

$$-(k_i \partial_{xx} u_{hi} + k_{xi} \partial_x u_{hi}) = f_i. \tag{36}$$

Here c_{1i}, c_{2i} can be determined by the interface conditions:

$$u_{hi}(x_i) = u_{hi+1}(x_i), \quad (\bar{K}_i \partial_x \bar{u}_{hi})|_{x_i} = (\bar{K}_{i+1} \partial_x \bar{u}_{hi+1})|_{x_i}. \tag{37}$$

Fig. 13 The stencil for 1D TFPM



That is

$$\begin{cases} \sum_{k=1}^2 c_{k,i} W_{k,i}(x) + \tilde{v}_i(x_i) = \sum_{k=1}^2 c_{k,i+1} W_{k,i+1}(x_i) + \tilde{v}_{i+1}(x_i), \\ \bar{K}_i(x_i) \left(\sum_{k=1}^2 c_{k,i} \partial_x W_{k,i} + \partial_x \tilde{v}_i \right) |_{x_i} = \bar{K}_{i+1}(x_{i+1}) \left(\sum_{k=1}^2 c_{k,i+1} \partial_x W_{k,i+1} + \partial_x \tilde{v}_{i+1} \right) |_{x_i}. \end{cases} \tag{38}$$

Combing the boundary conditions $u_{h1}(0) = u_0$, $u_{hI}(L) = u_L$ and interface conditions (38), we get a linear system of $2I$ equations and the coefficients c_{1i} , c_{2i} can be determined. Piecing together all u_{hi} , we find an approximation to the solution of (31).

Error Estimate for 1D TFPM

We give an L^2 error estimate for the above proposed 1D TFPM. We emphasis that the proof does not depend on the ration between $\max_i \{h_i\}$ and $\min_i \{h_i\}$. Assume that $h = \max_i \{h_i\}$. u satisfies (31), u_h is the solution to the 1D TFPM, then

$$\|u - u_h\|_2 = \left(\int_L |u - u_h|^2 dx \right)^{1/2} \leq \|u - \bar{u}\|_2 + \|\bar{u} - \bar{u}_h\|_2 + \|\bar{u}_h - u_h\|_2,$$

where

- $\bar{u} \in C^1[0, L]$ and satisfies (32) in each interval L_i . The boundary conditions are $\bar{u}(0) = u(0)$, $\bar{u}(L) = u(L)$.
- For all $i = 1, 2 \dots I$, $\bar{u}_h|_{L_i} = \bar{u}_{hi} = \sum_{k=1}^2 \bar{c}_{k,i} W_{k,i} + \tilde{v}_i$ with $W_{k,i}$, \tilde{v}_i being as in (35). $\bar{c}_{k,i}$ are constants that are determined by the following boundary conditions: $\partial_x \bar{u}_{hi}|_{x_i} = \partial_x \bar{u}_i|_{x_i}$, and $\bar{u}_{hi}(x_i) = \bar{u}_i(x_i)$.
- u_h is the solution to the 1D TFPM.

We prove that each of the three terms $\|u - \bar{u}\|_2$, $\|\bar{u} - \bar{u}_h\|_2$, $\|\bar{u}_h - u_h\|_2$ can be controlled by Ch^2 in the subsequent part.

Bound for $\|u - \bar{u}\|_2$

From the definitions of f_i and f_{xi} in (34), when $f(x)|_{L_i} \in C^2(L_i)$ for all $i \in \{1, \dots, I\}$, $f(x)|_{L_i} = \bar{f}_i + O(h_i^2)$. Then

$$\|f - \bar{f}\|_2^2 = \sum_{i=1}^I \int_{L_i} (f - \bar{f}_i)^2 dx \leq C \sum_{i=1}^I h_i^5 \leq CLh^4. \tag{39}$$

That is $\|f - \bar{f}\|_2 \leq Ch^2$. Similarly, $\|K - \bar{K}\|_2 < Ch^2$. We have the following lemma:

Lemma 1 Let $w = u - \bar{u}$, then

$$\|\partial_x w\|_2 < Ch^2, \quad \|w\|_2 < Ch^2, \tag{40}$$

where C is a constant independent of h .

Proof Multiplying both sides of Eq. (31) by w and integrating over $[0, L]$, from $w \in C^1[0, L]$ and $w(0) = w(L) = 0$, one gets

$$\int_L (\partial_x w) \cdot K \partial_x u dx = \int_L w f dx. \tag{41}$$

Similarly, from Eq. (32),

$$\int_L (\partial_x w) \cdot \bar{K} \partial_x \bar{u} \, dx = \int_L w \bar{f} \, dx. \tag{42}$$

Subtracting (42) from (41) yields

$$\begin{aligned} \zeta_1 \|\partial_x w\|_2^2 &\leq \int_\Omega (\partial_x w) \cdot K \partial_x w \, dx = - \int_L (\partial_x w) \cdot (K - \bar{K}) \partial_x \bar{u} \, dx + \int_L w(f - \bar{f}) \, dx \\ &\leq \|\partial_x w\|_2 \|(K - \bar{K}) \partial_x \bar{u}\|_2 + \|w\|_2 \|f - \bar{f}\|_2. \end{aligned} \tag{43}$$

where the last inequality is from Holder’s inequality. Since $w \in C^1[0, L]$, $w(0) = w(L) = 0$, from Friedrichs inequality we have $\|w\|_2 \leq C \|\partial_x w\|_2$. Therefore there exists C independent of h that satisfies

$$\|\partial_x w\|_2 \leq Ch^2.$$

Then Friedrichs inequality gives

$$\|w\|_2 \leq C \|\partial_x w\|_2 \leq Ch^2.$$

□

Bound for $\|\bar{u} - \bar{u}_h\|_2$

Let $u_h|_{L_i} = u_{hi}$, then \bar{u}_{hi} satisfies

$$(k_i \partial_{xx} \bar{u}_{hi} + k_{xi} \partial_x \bar{u}_{hi}) + f_i = 0, \tag{44}$$

Then

$$\partial_x \cdot (\bar{K}_i \partial_x \bar{u}_{hi}) + \bar{f}_i = R.H.S. \tag{45}$$

with

$$R.H.S. = k_{xi} \partial_x^2 \bar{u}_{hi}(x)(x - x_{i-1/2}) + f_{xi}(x - x_{i-1/2}). \tag{46}$$

Since $\frac{1}{h_i} \int_{L_i} x \, dx = x_{i-1/2}$ and $\bar{u}_{hi} \in C^\infty(L_i)$, we have

$$\int_{L_i} R.H.S. \, dx = \int_{L_i} k_{xi}(x - x_{i-1/2})(\partial_x^2 \bar{u}_{hi}(x_{i-1/2}) + (x - x_{i-1/2}) \partial_x^3 \bar{u}_{hi}(\xi(x))) \, dx = O(h_i^3). \tag{47}$$

The difference between \bar{u} and \bar{u}_h is given by the following lemma:

Lemma 2 Let $\bar{w} = \bar{u} - \bar{u}_h$, then $\bar{w}_i = \bar{w}|_{L_i} \in C^2(L_i)$ satisfies

$$\|\bar{w}_i\|_\infty \leq Ch_i^3, \quad |(\bar{K}_i \partial \bar{w}_i)|_{x_{i-1}}| \leq Ch_i^3.$$

where C is a constant independent of h_i .

Proof Since $\partial_x \bar{u}_{hi}|_{x_i} = \partial_x \bar{u}_i|_{x_i}$, $\bar{u}_{hi}(x_i) = \bar{u}_i(x_i)$, we have $\partial_x \bar{w}_i|_{x_i} = 0$, $\bar{w}_i(x_i) = 0$. It is easy to check that $\bar{w}_i \in C^2(L_i)$, then $\partial_x \bar{w}_i(x) = \partial_x \bar{w}_i(x_i) + (x - x_i) \partial_x^2 \bar{w}(\xi) = (x - x_i) \partial_x^2 \bar{w}(\xi)$ for some $\xi \in L_i$. (32) and (45) indicates that $\|k_i \partial_x^2 \bar{w}_i + k_{xi} \partial_x \bar{w}_i\|_{L^\infty} < Ch_i$, thus $\|\partial_x^2 \bar{w}_i\|_{L^\infty} < Ch_i$, and $\|\partial_x \bar{w}_i\|_{L^\infty} < Ch_i^2$. From $\bar{w}_i|_{x_i} = 0$, $\partial_x \bar{w}_i(x_i) = 0$, we have $\bar{w}_i = \bar{w}_i(x_i) + h_i \partial_x \bar{w}_i(x_i) + h_i^2 \partial_x^2 \bar{w}_i(\xi) = h_i^2 \partial_x^2 \bar{w}(\xi)$ and thus $\|\bar{w}_i\|_{L^\infty} < Ch_i^3$. On the other hand, (32) and (45) gives

$$\partial_x (\bar{K}_i \partial \bar{w}_i(x)) = -R.H.S. \tag{48}$$

Integrating over L_i we find

$$\bar{K}_i(x_i)\partial_x \bar{w}_i|_{x_i} - \bar{K}_i(x_{i-1})\partial_x \bar{w}_i|_{x_{i-1}} = O(h_i^3). \tag{49}$$

Together with $\partial_x \bar{w}_i|_{x_i} = 0$, we obtain

$$|(\bar{K}_i \partial_x \bar{w}_i)|_{x_{i-1}}| \leq Ch_i^3.$$

□

Bound for $\|\bar{u}_h - u_h\|_2$

The function values $\bar{u}_{hi}(x_i)$ and $\bar{u}_{hi+1}(x_i)$ are not necessarily the same. Since $\bar{u}_{i+1}(x_i) = \bar{u}_i(x_i)$ and $(\bar{K}_{i+1}\partial_x \bar{u}_{i+1})|_{x_i} = (\bar{K}_i\partial_x \bar{u}_i)|_{x_i}$, we have

$$\begin{aligned} & \bar{u}_{hi+1}(x_i) - \bar{u}_{hi}(x_i) \\ &= \bar{u}_{i+1}(x_i) - \bar{w}_{i+1}(x_i) - \bar{u}_i(x_i) + \bar{w}_i(x_i) = -\bar{w}_{i+1}(x_i) = O(h_{i+1}^3). \\ & (\bar{K}_{i+1}\partial_x \bar{u}_{i+1})|_{x_i} - (\bar{K}_i\partial_x \bar{u}_{hi})|_{x_i} \\ &= (\bar{K}_{i+1}\partial_x \bar{u}_{i+1})|_{x_i} - (\bar{K}_{i+1}\partial_x \bar{w}_{i+1})|_{x_i} - (\bar{K}_i\partial_x \bar{u}_i)|_{x_i} + (\bar{K}_i\partial_x \bar{w}_i)|_{x_i} = O(h_{i+1}^3). \end{aligned} \tag{50}$$

Then $\bar{u}_h|_{L_i} = \bar{u}_{hi} = \sum_{k=1}^2 \bar{c}_{k,i} W_{k,i} + \tilde{v}_i$ and satisfies the interface condition as in (50). At the boundary, $\bar{u}_{hi}(L) = u_L$, $\bar{u}_{h1}(0) = \bar{u}(0) - \bar{w}(0) = u_0 + O(h_1^3)$. The following lemma gives the distance between \bar{u}_h and u_h .

Lemma 3 *Let $w_h = \bar{u}_h - u_h$, then $w_{hi}(x) = w_h|_{L_i} \in C^\infty(L_i)$ and satisfies*

$$\|\partial_x w_h\|_\infty < Ch^2, \quad \|w_h\|_\infty \leq Ch^2,$$

where C is a constant independent of h .

Proof For $i = 1, \dots, I$, $k_i \partial_x^2 w_{hi} + k_{xi} \partial_x w_{hi} = 0$. From (37) and (50), for $i = 1, \dots, I - 1$,

$$w_{hi}(x_i) - w_{hi+1}(x_i) = O(h_{i+1}^3), \quad (\bar{K}_i \partial_x w_{hi})|_{x_i} - (\bar{K}_{i+1} \partial_x w_{hi+1})|_{x_i} = O(h_{i+1}^3). \tag{51}$$

At the boundary $w_h(L) = 0$, $w_h(0) = O(h_1^3)$. First of all, we show that there exists $\xi \in [0, L]$ such that $|\partial_x w_h(\xi)| \leq Ch^2$. There are three situations:

- For some $j \in \{1, 2, \dots, I\}$, there exists $\xi \in (x_{j-1}, x_j)$ such that $\partial_x w_{hj}(\xi) = 0$.
- For any given $j \in \{1, \dots, I\}$, $\forall x \in L_j$, $\partial_x w_{hj}(x)$ has the same sign, and there exists $j \in \{1, \dots, I - 1\}$ such that

$$\partial_x w_{hj}(x_j)\partial_x w_{hj+1}(x_j) \leq 0.$$

From (51) and the fact that $\bar{K}_i(x_i) = \bar{K}_{i+1}(x_i) > 0$, we find

$$|\partial_x w_{hj}(x_j)| \leq Ch_{i+1}^3$$

- For any given $j \in \{1, \dots, I\}$, $\forall x \in L_j$, $\partial_x w_{hj}(x)$ has the same sign and for all $j \in \{1, \dots, I - 1\}$

$$\partial_x w_{hj}(x_j)\partial_x w_{hj+1}(x_j) \geq 0.$$

Assume that for $\forall i \in \{1, \dots, I - 1\}$, $\partial_x w_{hi}(x_i) \geq 0$, $\partial_x w_{hi+1}(x_i) \geq 0$, then $w_{hi}(x_i) \geq w_{hi}(x_{i-1})$ for $\forall i \in \{1, \dots, I\}$ and

$$\left| \sum_{i=1}^I (w_{hi}(x_i) - w_{hi}(x_{i-1})) \right| \geq \min_{i=1, \dots, I} |\partial_x w_{hi}(\xi_i)| \sum_{i=1}^I h_i,$$

where $\xi_i \in L_i$ and satisfies $w_{hi}(x_i) - w_{hi}(x_{i-1}) = h_i \partial_x w_{hi}(\xi_i)$. On the other hand,

$$\begin{aligned} \left| \sum_{i=1}^I \int_{L_i} \partial_x w_h \, dx \right| &= \left| \sum_{i=1}^I (w_{hi}(x_i) - w_{hi}(x_{i-1})) \right| \\ &= \left| \sum_{i=1}^{I-1} (w_{hi}(x_i) - w_{hi+1}(x_i)) - w_{h1}(0) + w_{hI}(L) \right| \\ &\leq C \sum_{i=1}^I h_i^3. \end{aligned}$$

Similar results hold when $\forall i \in \{1, \dots, I - 1\}$, $\partial_x w_{hi}(x_i) \leq 0$, $\partial_x w_{hi+1}(x_i) \leq 0$. Thus

$$\min_{i=1, \dots, I} |\partial_x w_{hi}(\xi_i)| < Ch^2$$

We have shown that there exists $\xi \in L_s$, such that $|\partial_x w_h(\xi)| \leq Ch^2$, we then prove by induction that $\forall x \in [0, L]$, $|\partial_x w_h(x)| < Ch^2$. We first consider the interval $[\xi, x_s]$. Since $|\partial_x w_h(\xi)| \leq Ch^2$ and $k_s \partial_x^2 w_h(\xi) + k_{x_s} \partial_x w_h(\xi) = 0$, we have $|\partial_x^2 w_h(\xi)| \leq Ch^2$. Let

$$\alpha = \frac{|k_{x_s}|}{|k_s|},$$

then for $\forall x \in [\xi, x_s]$,

$$\begin{aligned} |\partial_x^2 w_{hs}(x)| &= \alpha |\partial_x w_h(x)| \leq \alpha \left| \partial_x w_{hs}(\xi) + (x - \xi) \partial_x^2 w_{hs}(\xi') \right| \\ &\leq \alpha \left| \partial_x w_{hs}(\xi) - (x - \xi) \alpha \partial_x w_{hs}(\xi') \right| \\ &\leq Ch^2 \end{aligned}$$

where $\xi' \in [\xi, x]$. Then for $\forall x \in [\xi, x_s]$,

$$\begin{aligned} |\partial_x w_{hs}(x)| &= \left| \partial_x w_{hs}(\xi) + (x - \xi) \partial_x^2 w_{hs}(\xi) + \frac{1}{2} (x - \xi)^2 \partial_x^3 w_{hs}(\eta_s) \right| \\ &= \left| \partial_x w_{hs}(\xi) + (x - \xi) \partial_x^2 w_{hs}(\xi) - \frac{1}{2} (x - \xi)^2 \alpha \partial_x^2 w_{hs}(\eta_s) \right| \\ &< Ch^2 (1 + h_s \alpha + h_s^2 \alpha), \end{aligned}$$

where we have used $k_s \partial_x^3 w_h(\eta_s) + k_{x_s} \partial_x^2 w_h(\eta_s) = 0$ in the second equality. Since $\bar{K}_s(x_s) = \bar{K}_{s+1}(x_s)$, we have $\partial_x w_{hs}(x_s) - \partial_x w_{hs+1}(x_s) = O(h_{s+1}^3)$ from (51), then

$$|\partial_x w_{hs+1}(x_s)| < Ch^2 (1 + h_s \alpha + h_s^2 \alpha) + Ch_{s+1}^3.$$

Similar discussions for the interval L_{s+1} , we get

$$\begin{aligned} |\partial_x w_{hs+1}(x_{s+1})| &= \left| \partial_x w_{hs+1}(x_s) + (x - x_s) \partial_x^2 w_{hs+1}(x_s) + \frac{1}{2} (x - x_s)^2 \partial_x^3 w_{hs+1}(\eta_{s+1}) \right| \\ &\leq \left(Ch^2 (1 + \alpha h_s + h_s^2 \alpha) + Ch_{s+1}^3 \right) (1 + h_{s+1} \alpha + h_{s+1}^2 \alpha) \end{aligned}$$

and

$$|\partial_x w_{hs+2}(x_{s+1})| \leq \left(Ch^2 (1 + \alpha h_s + h_s^2 \alpha) + Ch_{s+1}^3 \right) (1 + h_{s+1} \alpha + h_{s+1}^2 \alpha) + Ch_{s+2}^3$$

By induction, we find for $\forall s' \in \{s + 1, \dots, I\}$ and $\forall x \in L_{s'}$,

$$\begin{aligned}
 |\partial_x w_{h_{s'}}(x)| \leq & Ch^2 \Pi_{i=s}^{s'} (1 + h_i \alpha + h_i^2 \alpha) + Ch_{s+1}^3 \Pi_{i=s+1}^{s'} (1 + h_i \alpha + h_i^2 \alpha) \\
 & + Ch_{s'}^3 (1 + h_{s'} \alpha + h_{s'}^2 \alpha)
 \end{aligned} \tag{52}$$

Since the geometrical mean is less than the arithmetic mean, we have for arbitrary $s_1, s_2 \in \{s, s + 1, \dots, I\}$ and $s_1 < s_2$,

$$\Pi_{i=s_1}^{s_2} (1 + h_i \alpha + h_i^2 \alpha) \leq \left(\frac{\sum_{i=s_1}^{s_2} (1 + h_i \alpha + h_i^2 \alpha)}{s_2 - s_1} \right)^{s_2 - s_1} \leq \left(1 + \frac{CL}{s_2 - s_1} \right)^{s_2 - s_1} \leq C$$

where C is a constants independent of I and h_i . Then (52) gives that for $\forall x \in [\xi, L]$, $|\partial_x w_h(x)| < Ch^2$. Similar result holds for the interval $[0, \xi]$ and we find $\|\partial_x w_h\|_\infty \leq Ch^2$. Then since $w_h(L) = 0$, it is easy to check $\|w_h\|_\infty \leq Ch^2$ by induction. \square

References

1. Ashby, S.F., Bosl, W.J., Falgout, R.D., Smith, S.G., Tompson, A.F., Williams, T.J.: A numerical simulation of groundwater flow and contaminant transport on the CRAY T3D and C90 Supercomputers. *Int. J. High Perform. Comput. Appl.* **13**(1), 80–93 (1999)
2. van Esa, Bram, Koren, Barry, de Blank, Hugo J.: Finite-difference schemes for anisotropic diffusion. *J. Comput. Phys.* **272**, 526–549 (2014)
3. Günter, S., Yu, Q., Krüger, J. et al.: Modelling of heat transport in magnetised plasmas using non-aligned coordinates. *J. Comput. Phys.*, 209 (2005) 354–370
4. Galperin, B., Sukoriansky, S.: Geophysical flows with anisotropic turbulence and dispersive waves: flows with stable stratification. *Ocean Dyn.* **60**, 1319–1337 (2010)
5. Yuan, G.W., Sheng, Z.Q.: Monotone finite volume schemes for diffusion equations on polygonal meshes. *J. Comput. Phys.* **227**(12), 6288–6312 (2008)
6. Barth, T.J., Ohlberger, M.: Finite volume methods: foundation and analysis E. Stein, R. de Borst, T. Huges (Eds.), *Encyclopedia of Computational Mechanics*, John Wiley and Sons Ltd. (2004)
7. Droniou, J.: Finite volume schemes for diffusion equations: introduction to and review of modern methods. *Math. Models Methods Appl. Sci.* **24**(8), 1575–1619 (2014)
8. Herbin, R., Hubert, F.: Benchmark on Discretization Schemes for Anisotropic Diffusion Problems on General Grids. *Finite volumes for complex applications V, France* (2008)
9. Droniou, J., Eymard, R.: A mixed finite volume scheme for anisotropic diffusion problems on any grid. *Numer. Math.* **105**(1), 35–71 (2006)
10. Edwards, M.G., Rogers, C.F.: Finite volume discretization with imposed flux continuity for the general tensor pressure equation. *Comput. Geosci.* **2**, 259–290 (1998)
11. Eymard, R., Gallouët, T., Herbin, R.: A cell-centred finite-volume approximation for anisotropic diffusion operators on unstructured meshes in any space dimension, *IMA J. Numer. Anal.* **26** (2006) 326–353
12. Eymard, R., Gallouët, T., Herbin, R.: Discretization of heterogeneous and anisotropic diffusion problems on general nonconforming meshes, *SUSHI: a scheme using stabilization and hybrid interfaces*, *IMA J. Numer. Anal.* **30** (4), (2010) 1009–1043
13. Lipnikov, K., Shashkov, M., Svyatskiy, D., Vassilevski, Yu.: Monotone finite volume schemes for diffusion equations on unstructured triangular and shape-regular polygonal meshes regimes. *J. Comput. Phys.* **227**, 492–512 (2007)
14. Lipnikov, K., Svyatskiy, D., Vassilevski, Y.: A monotone finite volume method for advection-diffusion equations on unstructured polygonal meshes. *J. Comput. Phys.* **229**, 4017–4032 (2010)
15. Sheng, Z.Q., Yue, J.Y., Yuan, G.W.: Monotone finite volume schemes of nonequilibrium radiation diffusion equations on distorted meshes. *SIAM J. Sci. Comput.* **31**(4), 2915–2934 (2009)
16. Sheng, Z.Q., Yuan, G.W.: A new nonlinear finite volume scheme preserving positivity for diffusion equations. *J. Comput. Phys.* **315**, 182–193 (2016)
17. Wu, J., Gao, Z.: Interpolation-based second-order monotone finite volume schemes for anisotropic diffusion equations on general grids. *J. Comput. Phys.* **275**, 569–588 (2014)
18. Arnold, D.N.: An interior penalty finite element method with discontinuous elements. *SIAM J. Numer. Anal.* **19**, 742–760 (1982)

19. Ern, A., Stephansen, A.F., Zunino, P.: A discontinuous Galerkin method with weighted averages for advection-diffusion equations with locally small and anisotropic diffusivity. *IMA J. Numer. Anal.* **29**, 235–256 (2009)
20. Zhang, X.P., Su, S., Wu, J.M.: A vertex-centered and positivity-preserving scheme for anisotropic diffusion problems on arbitrary polygonal grids. *J. Comput. Phys.* **344**, 419–436 (2017)
21. Arnold, D.N., Boffi, D., Falk, R.S., Gastaldi, L.: Finite element approximation on quadrilateral meshes. *Comm. Numer. Methods Engrg.* **17**, 805–812 (2001)
22. Arnold, D.N., Boffi, D., Falk, R.S.: Approximation by quadrilateral finite elements. *Math. Comp.* **239**, 909–922 (2002)
23. Hou, T.Y., Wu, X.H.: A multiscale finite element method for elliptic problems in composite materials and porous media. *J. Comput. Phys.* **134**, 169–189 (1997)
24. Li, X., Huang, W.: An anisotropic mesh adaptation method for the finite element solution of heterogeneous anisotropic diffusion problems. *J. Comput. Phys.* **229**, 8072–8094 (2010)
25. Pasdunkorale, J., Turner, I.W.: A second order control-volume finite-element least-squares strategy for simulating diffusion in strongly anisotropic media. *J. Comput. Math.* **23**, 1–16 (2005)
26. Rajendran, S.: A technique to develop mesh-distortion immune finite elements. *Comput. Methods Appl. Mech. Eng.* **199**, 1044–1063 (2010)
27. Cen, S., Zhou, M. J., Shang, Y.: Shape-Free Finite Element Method: Another Way between Mesh and Mesh-Free Methods, *Math. Probl. Eng.* (2013) Article ID 491626
28. Kuznetsov, Y., Repin, S.: Convergence analysis and error estimates for mixed finite element method on distorted meshes. *J. Numer. Math.* **13**(1), 33–51 (2005)
29. Droniou, J., Eymard, R., Gallout, T., Herbin, R.: A unified approach to mimetic finite difference, hybrid finite volume and mixed finite volume methods. *Math. Models. Meth. Appl. Sci.* **20**(2), 265–295 (2008)
30. Günter, S., Lackner, K.: A mixed implicit-explicit finite difference scheme for heat transport in magnetised plasmas. *J. Comput. Phys.*, 2 (2009) 282–293
31. Gyrya, V., Lipnikov, K.: The arbitrary order mimetic finite difference method for a diffusion equation with a non-symmetric diffusion tensor. *J. Comput. Phys.* **348**, 549–566 (2017)
32. Hyman, J., Shashkov, M., Steinberg, S.: The numerical solution of diffusion problems in strongly heterogeneous non-isotropic materials. *J. Comput. Phys.* **132**, 130–148 (1997)
33. Hyman, J., Morel, J., Shashkov, M., Steinberg, S.: Mimetic finite difference methods for diffusion equations. *Comput. Geosci.* **6**, 333–352 (2002)
34. Han, H., Huang, Z., Kellogg, B.: A Tailored finite point method for a singular perturbation problem on an unbounded domain. *J. Sci. Comp.* **36**, 243–261 (2008)
35. Han, H., Huang, Z.Y.: Tailored finite point method for a singular perturbation problem with variable coefficients in two dimensions. *J. Sci. Comput.* **49**, 200–220 (2009)
36. Han, H., Huang, Z.Y.: Tailored finite point method for steady-state reaction-diffusion equation. *Commun. Math. Sci.* **8**, 887–899 (2010)
37. Han, H., Huang, Z.Y.: Tailored finite point method based on exponential bases for convection-diffusion-reaction equation. *Math. Comput.* **82**, 213–226 (2013)
38. Han, H., Huang, Z.Y., Ying, W.J.: A Semi-discrete tailored finite point method for a class of anisotropic diffusion problems. *Comput. Math. Appl.* **65**, 1760–1774 (2013)
39. Huang, Z., Li, Y.: Monotone finite point method for non-equilibrium radiation diffusion equations. *BIT Numer. Math.* **56**, 659–679 (2016)
40. Huang, Z., Yang, Y.: Tailored finite point method for parabolic problems. *Comput. Meth. Appl. Math.* **16**, 543–562 (2016)
41. Tang, M., Wang, Y.H.: Uniform convergent tailored finite point method for advection-diffusion equation with discontinuous, anisotropic and vanishing diffusivity. *J. Sci. Comput.* **70**(1), 272–300 (2017)
42. Breil, J., Maire, P.H.: A cell-centered diffusion scheme on two-dimensional unstructured meshes. *J. Comput. Phys.* **224**, 785–823 (2007)
43. Shashkov, M., Steinberg, S.: Solving diffusion equations with rough coefficients in rough grids. *J. Comp. Phys.* **129**, 383–405 (1996)
44. Cheng, K., Feng, W., Wang, C., Wise, S.M.: An energy stable fourth order finite difference scheme for the Cahn-Hilliard equation. *J. Comput. Appl. Math.* **362**, 574–595 (2019)
45. Liu, J.G., Wang, C., Johnston, H.: A fourth order scheme for incompressible boussinesq equations. *J. Sci. Comput.* **18**(2), 253–285 (2003)